Constraining the mechanisms of aeolian bedform formation on Mars through a global morphometric survey

David A. Vaz[1], Simone Silvestro[2,3], Matthew Chojnacki[4] and David C. A. Silva[1]

[1] Centre for Earth and Space Research of the University of Coimbra, Observatório Geofísico e Astronómico da Universidade de Coimbra, Coimbra, Portugal.

[2] INAF Osservatorio Astronomico di Capodimonte, Napoli, Italia.

[3] SETI Institute, Carl Sagan Center, Mountain View, CA, USA.

[4] Planetary Science Institute, Lakewood, CO, USA.

Corresponding author: David Vaz (davidvaz@uc.pt)

Key Points:

- We present a global morphometric survey of aeolian bedforms on Mars and assess the mechanisms that may control their size
- Bedforms within the high elevation Tharsis region form a distinct group, attributed here to different sediment and transport conditions
- We confirm the existence of a robust relation between wavelength and atmospheric density, which is consistent with a fluid-drag mechanism

Abstract

Aeolian processes on Mars form a distinct class of meter-scale ripples, whose mechanisms of formation are debated. We present a global morphometric survey of bedforms on Mars, adding relevant observational constraints to the ongoing debate. We show that the bedforms located in the Tharsis region form a distinct group, not akin to the large dark-toned ripples which cover dune fields elsewhere on the planet. The relation between wavelength and atmospheric density derived from the new data is consistent with the predictions of a wind-drag mechanism, favoring the model that uses a saltation saturation length. Regardless of the mechanism that limits the size of bedforms, these results confirm the existence of a robust relationship between the wavelength of large ripples and atmospheric density (ripples spacings increases with decreasing atmospheric density). This provides further support to the interpretation of paleoatmospheric conditions on Mars through the analysis of its aeolian sedimentary record.

Plain Language Summary

The winds that shape the surface of Mars form two distinct scales of aeolian ripples, which coexist and evolve over martian dunes. The larger ripples (with spacing between crests between 1-5 m) are enigmatic, as the mechanisms that control their equilibrium size are not fully understood. In this study we provide new observational data, which we use to assess different models that predict a dependence of bedform wavelength with atmospheric density. This new dataset shows that there are more than one population of meter-scale bedforms, with the ones located around the Tharsis volcanos being significantly different from the ones that cover dark dunes. We found a good agreement with the predictions of the wind-drag model, suggesting that the size of the large ripples is controlled by an aerodynamic mechanism. Most importantly, we confirm the existence of a global relation between wavelength and atmospheric density (ripples spacings increases with decreasing atmospheric density). This provides further support to the interpretation of paleoatmospheric conditions on Mars, as this relation can be applied to infer past atmospheric densities from the sedimentary record.

1 Introduction

Martian dark dunes are covered by large ripple-like bedforms which are actively migrating under present-day atmospheric conditions (Bridges et al., 2012; Silvestro et al., 2010). These are metric-scale bedforms (~1-5 m spacing between crests, ~5-40 cm high) which can have symmetrical or asymmetrical profiles and sinuous or straight crests. On terrestrial aeolian environments with well-sorted sediments there are no obvious analogue bedforms in terms of scale, morphometry and dynamics (Lapotre et al., 2018; Silvestro et al., 2016; Vaz et al., 2017). Most notably, the meter-scale bedform are overlaid by centimeter-scale ripples, similar in scale and dynamics to impact ripples (Bridges et al., 2012; Lapotre et al., 2016; Weitz et al., 2018). The coexistence to these two different scales of bedforms raised several questions. Namely, why do we have two scales of ripples on Mars and what are the mechanisms that control their sizes?

To explain orbital and ground-based observations of widespread aeolian activity (Baker et al., 2022; Bridges et al., 2012; Silvestro et al., 2010, 2013) transient low-flux transport regimes, that occur between impact threshold and fluid threshold speeds, were invoked (Andreotti et al., 2021; Baker et al., 2018; Lapotre et al., 2018; Sullivan & Kok, 2017; Swann et al., 2020). Recent in situ observations by the Curiosity rover at Gale crater demonstrate that intermittent saltation is taking place, contributing to the migration of centimeter-scale ripples (Baker et al., 2022; Sullivan et al., 2022). In addition, wind tunnel experiments suggest that the size of impact ripples does not vary significantly with atmospheric density, maintaining their characteristic centimeter scale even in the low density conditions that exist on the surface of Mars (Andreotti et al., 2021). Therefore, all evidence shows that the size of centimeter scale ripples on Mars is controlled by the same impact-splash mechanism that produces terrestrial aeolian impact ripples.

In contrast, two hypotheses have been proposed to explain the origin of the meter-scale ripples. They have been interpreted: a) as arising from a hydrodynamic instability i.e., they are analogous to fluid drag ripples typically found on terrestrial subaqueous environments (Duran Vinent et al., 2019; Lapotre et al., 2016, 2021); or b) as forming from the same impact-splash mechanism as terrestrial aeolian ripples (Sullivan et al., 2020; Sullivan & Kok, 2017). In the first hypothesis, the equilibrium wavelength of the large ripples is limited by a hydrodynamic anomaly (Duran Vinent et al., 2019; Lapotre et al., 2016), while in the second case ripple height (and consequently their wavelength) is controlled by the wind dynamic pressure at the bedforms crests, which is lower on Mars and would allow the growth of the bedforms (Sullivan et al., 2020). Lapotre et al. (2016, 2021) argued that there is a clear wavelength gap between the two types of bedforms, inferring that two different mechanisms are limiting the size of the bedforms (impact-splash for the centimeter-scale ripples and fluid-drag for the meter-scale bedforms). In contrast, Sullivan et al. (2022) reported a continuum distribution of superimposed ripple wavelengths observed by the Curiosity rover at the "Sands of Forvie" sand sheet. They also reported the existence of granulometric segregation between the troughs and crests of large ripples (the same was reported in other areas by Gough et al., 2021) with coarser grains preferentially located on the crests of the larger bedforms. They interpreted these two characteristics as evidence that the meter-scale ripples are impact ripples rather than fluid-drag bedforms.

An important aspect of the debate about the mechanism that sets the size of large ripples is the near-inverse relation observed between wavelength and atmospheric density at a global scale. This relation was initially hinted at by Lorenz et al. (2014) for the bedforms located across the high elevation Tharsis region, while Lapotre et al. (2016) extended the number of surveyed areas, focusing on sites where dark dunes are present. Based on this compilation, Lapotre et al. (2016) argued that the observed decrease in ripple wavelength with increasing atmospheric density is consistent with a fluid-drag origin. A view not shared by Lorenz (2020), which highlighted the different gradient of the model predictions and observational data (see Fig. 2 in Lorenz, 2020). Lapotre et al. (2021) revisited the same dataset proposing that when a saltation saturation length formulation is adopted (Duran Vinent et al., 2019), the fluid-drag mechanism provides a better fit to the data, particularly to the bedforms analyzed outside Tharsis.

Drag ripples wavelength scales according to $\lambda \approx \frac{\left(\frac{\mu}{\rho_f}\right)^{2/3} D^{1/6}}{(Rg)^{1/6} u_*^{1/3}}$ (Lapotre et al., 2017), where μ is the dynamic viscosity, ρ_f is the fluid density, D is grain diameter, g is the gravity acceleration and R is the submerged reduced density of the sediment ($\frac{\rho_s - \rho_f}{\rho_f}$). This relation predicts that bedform wavelength is strongly dependent on ${\rho_f}^{-2/3}$. The mechanisms that set the wavelength of impact ripples are less understood. Wind tunnel experiments show that the saturation wavelength on well sorted sediments increases linearly with friction velocity (Andreotti et al., 2006; Cheng et al., 2018; Rasmussen et al., 2015), and is thought to be limited by the height of the ripples (Bagnold, 1954; Manukyan & Prigozhin, 2009). Yet, in less well sorted sediments coarser particles form an armor layer on the crests, causing ripples to increase in height and consequently in wavelength (Sharp, 1963). Sullivan et al. (2020) argue that the wind dynamic pressure $WDP = \frac{1}{2}\rho_f u^2$ (u is the wind velocity) controls ripples height, with higher dynamic pressures removing particles from the crests and precluding the growth of the bedforms. Therefore, higher WDP should generate smaller ripples. In this case, if we assume a constant wind velocity the wavelength of impact ripples scales with $1/\rho_f$. Note that this assumption (constant wind speed at a global scale) may be problematic, as according to the equation WDP may be relatively more influenced by wind velocity than by density variations, which is the only factor addressed in previous studies as well as in this work. Nevertheless, both theories suggest an increase in wavelength when atmospheric density decreases.

Other questions not entirely settled in previous studies regard the nature of the bedforms located in the Tharsis region. Lapotre et al. (2016) noticed the morphologic and albedo differences between the dark-toned ripples covering dunes and Tharsis bedforms. Nevertheless, they merged the two datasets to fit their wind-drag model, while in later works Tharsis and non-Tharsis bedforms were analyzed separately (Lapotre et al., 2021; Lorenz, 2020).

Here we focus on these unresolved issues, reviewing and expanding the observational dataset, analyzing the consistency of measurements, and testing the models that predict the size of large ripples on Mars as a function of atmospheric density.

2 Data and methodology

We use High-Resolution Imaging Science Experiment (HiRISE) images (0.25-0.5 m/pix, McEwen et al., 2007) to perform a global scale mapping and wavelength survey of aeolian bedforms. Our survey cover the same 25 areas located in the Tharsis regions and analyzed by Lorenz et al. (2014), as well as the 11 areas reported in Lapotre et al. (2016) (Fig. 1). Furthermore, we expand the elevation coverage including 39 new areas where meter-scale bedforms are present covering dark-toned dunes (Supporting information S1 - section 1, Fig. S1 and Table S1).

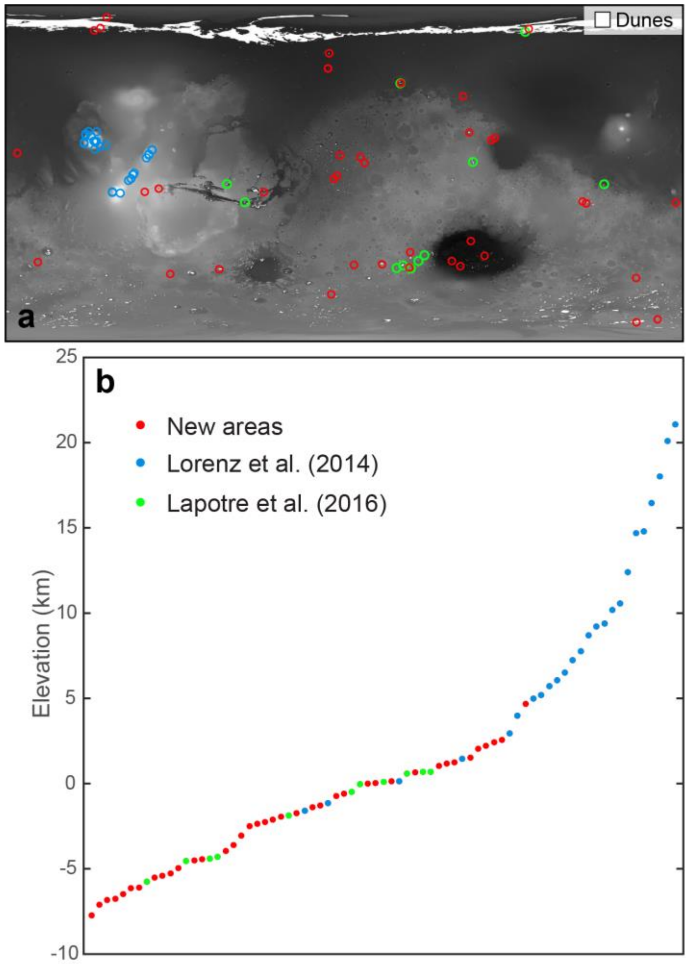

Figure 1. Location (a) and elevation distribution (b) of the 75 sites surveyed in this study. We analyzed the same 25 areas of Lorenz et al. (2014) as well as the 11 dark-tone dune sites previously analyzed by Lapotre et al. (2016). Our survey improves the spatial coverage, extends the range of surveyed elevations and provides a more continuous elevation sampling. A global dune catalog (Fenton, 2020; Hayward et al., 2014) is shown overlaying MOLA elevation data.

Previous surveys relied on the discrete manual measurements of crest-to-crest distances in randomly selected points (Lapotre et al., 2016; Lorenz et al., 2014). Here we applied a set of image processing and machine learning techniques which allow the mass automatic mapping of bedforms and the accurate measurement of their wavelengths (Fig. 2). We adapted the 2D Fast Fourier Transform approach introduced by Voulgaris and Morin (2008), implementing a multiscale scheme coupled with neural networks. This method allows the mapping and characterization of large ripples and transverse aeolian ridges (TARs) in a wide range of spatial scales and surface settings. See Supporting information S1 - section 2 for a in depth description of the method.

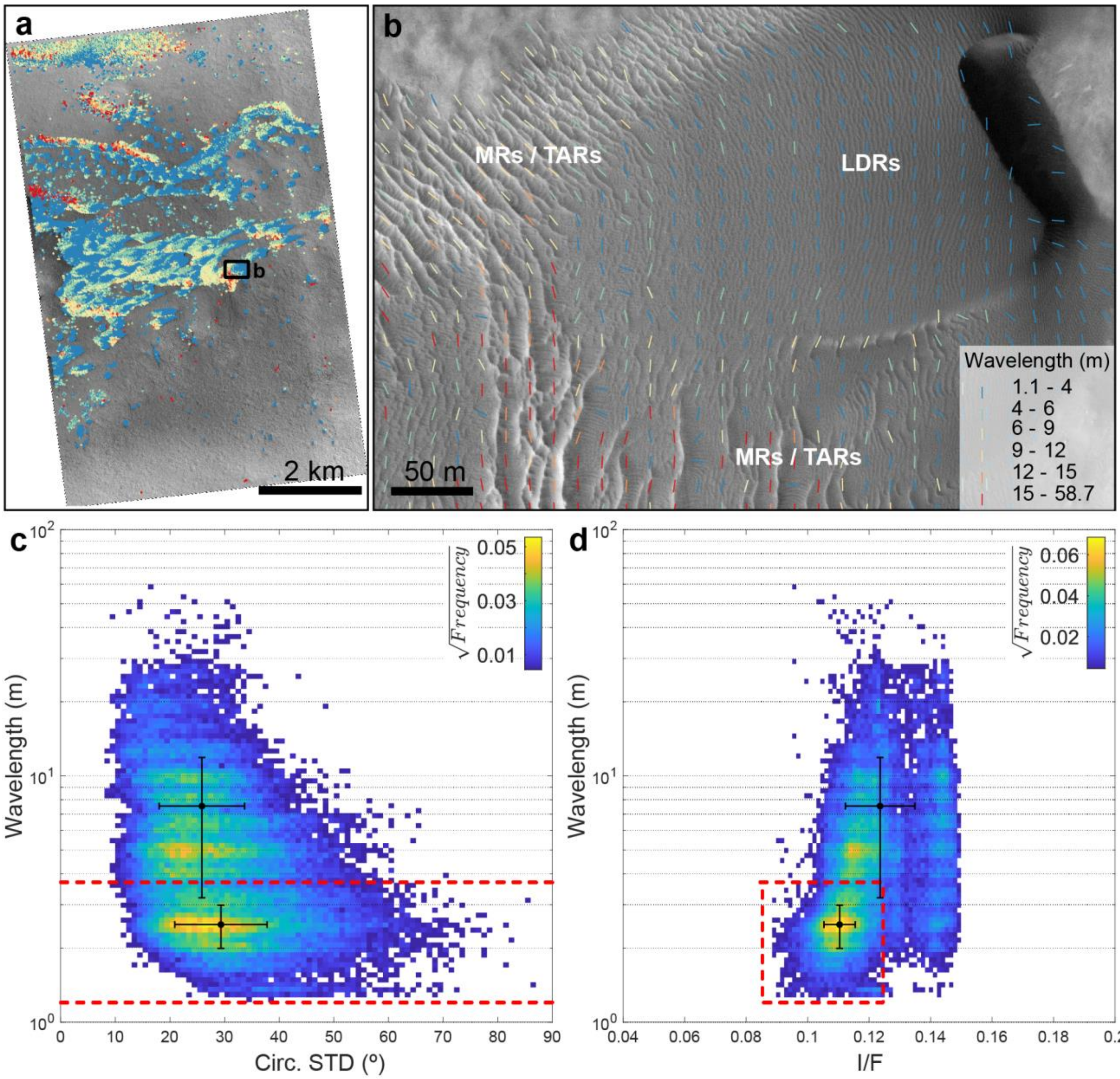

Figure 2. Wavelength survey of aeolian bedforms on Lyot crater (ESP_055318_2290, area 26 in Table S1). a) The applied method allows the full mapping and wavelength characterization of aeolian bedforms. b) Detailed view of the wavelength and trend of the mapped bedforms: large dark-toned ripples (LDRs) cover a barchan dune and have a spacing between crests of less than 4 m; megaripples (MRs) and transverse aeolian ridges (TARs) present higher albedos, higher wavelengths and are overlaid by the dune darker sediments. c and d) 2D histograms showing the

distribution of wavelength, circular standard deviation and albedo (I/F), a square root stretch is used to highlight secondary peaks. Red dashed lines correspond to the wavelength and albedo thresholds used to segment two bedform classes. The black dots and lines represent the computed averages and 1σ intervals.

Previous studies analyzed the relation between the average wavelength and atmospheric density at the surface, focusing on large ripples and TARs. To comply with this framework, we segment the mapped bedforms in two classes: a) large dark-toned ripples and b) a second class that comprises megaripples and TARs. Wavelength and relative grain size were proposed to be key parameters to discriminate different types of aeolian bedforms on Mars (Day & Zimbelman, 2021). We use albedo as a proxy for grain size, as it is usually assumed to be related to dust coating and/or to the presence of coarser particles (Sullivan et al., 2020). We examine the wavelength and albedo distributions using 2D histograms and we define threshold values that allow the partition of the mapping results, so that summary statistics can be computed for each class (see Supporting information S1 - section 3 for examples and Supporting information S2 for global results).

To evaluate the mechanisms that set the size of large ripples on Mars we test which model best describes the wavelength vs. atmospheric density relation observed in our dataset. We tested three models (refer to Supporting information S1 - section 5 for details): a) the wind-drag model of Lapotre et al. (2016), where the saturation length scale is approximated as that of fluvial bedload, b) a modified version of the same scaling, which instead uses a saturation length scale for aeolian saltation (Duran Vinent et al., 2019; Lapotre et al., 2021), and c) a generic inverse linear dependence between wavelength and atmospheric density (as proposed by Lorenz et al., 2014). We fit power laws and linear models to facilitate the comparison between our measurements and the models' predictions.

4 Results and discussion

Bedforms spaced between 1 to 100 m were mapped over a total area of ~2200 km^2 (Supporting information S2). The applied method correctly identifies the location of bedforms (93.7% of overall accuracy) and robustly measures their wavelength (we estimate a confidence interval of ±12%, Supporting information S1 - section 2). When comparing our data with previous surveys, we found a good agreement with large ripple measurements reported by Lapotre et al. (2016), which on average differ by 4%. Yet, the averages for the larger bedforms (megaripples and TARs) reported in the same study are severely underestimated by 84%, which we attribute to a possible under sampling. To assess the wavelength of these larger bedforms Lapotre et al. (2016) collected on average of 46 wavelength measurements on each site. This number of randomly located measurements may not be enough to characterize these populations, as they cover a small percentage of the mapped areas and form scattered patches of bedforms with variable wavelengths.

Our results for the Tharsis sites (which represent ~2/3 of the data analyzed in previous studies) show that Lorenz et al. (2014) values are systematically underestimated: on average they are 73% lower than the values obtained in this study (Fig. S10 and S11; Supporting information S1 - section 4). Indeed, some cited measurements there (e.g., 0.5-1.1 m) are dubious at best given HiRISE resolution (0.25 m/pix). The causes for this large disparity are less clear, nevertheless we note that in this case the measurement locations were not randomized, and that in some of the areas the spatial distribution of the bedforms is not uniform. These two factors may complicate the obtention of representative values from a few tens of scattered measurements.

Other potential sources of uncertainty are the elevation values reported for each site, which are used to derive the atmospheric pressure. We sampled the MOLA elevations at the centroid point of the largest bedform patch mapped in each area. However, previous works do not refer the sampling scheme or location where elevation values were collected. Therefore, in areas where the HiRISE footprints cover regions with higher elevation gradients (mainly in the Tharsis region) we can have elevation differences between our values and previous surveys of more than 2 km. This happens in four of the areas analyzed by Lorenz et al. (2014) (Fig. S11b).

We found several lines of evidence which support that Tharsis bedforms form a distinct population, apart from the large dark-toned ripples found elsewhere on Mars: a) as noted by Lapotre et al. (2021), we found that Tharsis bedforms have higher albedos (Fig. S12); b) we found that they have distinct thermal inertia (Putzig and Mellon, 2007) and dust cover index signatures (Ruff and Christensen, 2002), denoting lower thermal inertias (possibly associated with finer materials) and higher dust content/coverage (Fig. S13); c) as noted by others, Tharsis bedforms form unique patterns (Fig. S14) such as honeycomb or reticulate patterns (Bridges et al., 2010; Lorenz et al., 2014); and d) are in most cases associated with extensive mantling units, while large ripples outside Tharsis are typically found overlaying dark dunes (see Supporting information S1

- section 5 for details). These distinctive characteristics suggest that the two sets of bedforms should be considered separately when evaluating bedform-formation mechanisms.

The compiled data confirms the existence of a decrease of wavelength with increasing atmospheric density for the large dark-toned ripples (Fig. 3). Only five areas (~7%) deviate from this general tendency (Supporting information S1 - section 5 and Fig. S15), corresponding to cases where: a) sand sheets occupy a significant percentage of the mapped areas, suggesting the presence of coarse and/or poorly sorted sediments; and b) where dust devil tracks are visible covering the bedforms, suggesting limited migration/activity. These outliers are not included in the fits done to evaluate the proposed models, but their existence highlights two points: the accuracy and consistency of the measurements and the need to select comparable dune settings, as differences in grain size and sorting influence the wavelength of the bedforms.

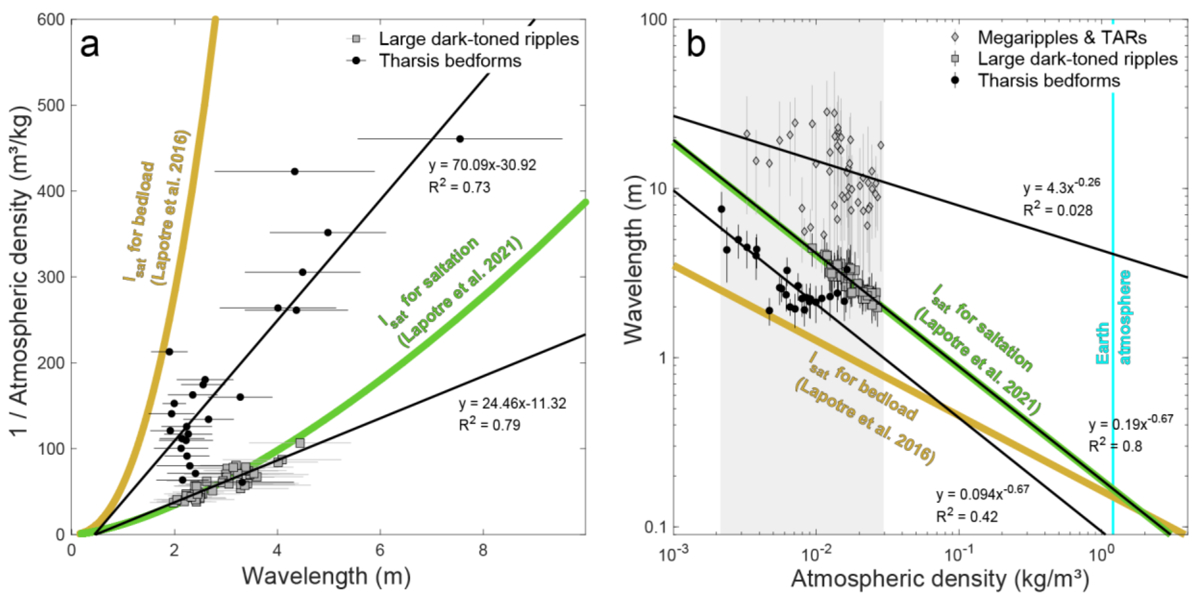

Figure 3. Relation between bedforms wavelength and Martian atmospheric density. The same data is shown in two different plots: a) highlighting the linear inverse relation proposed by Lorenz et al. (2014) and b) comparing with the models proposed by Lapotre et al. (2016; 2021), the gray area represents the maximum range of atmospheric densities on Mars while the cyan line represents the density of Earth's atmosphere. Black lines represent the best fitted models for each dataset, computed using the average wavelengths for each site (linear models in a) and power laws in b); the R^2 values in b) were computed in the log space). The golden line represents Lapotre et al. (2016) empirical relationship where transport saturation length is taken as that of fluvial bedload,

while the green line corresponds to a transport saturation length for aeolian saltation (Lapotre et al., 2021). A similar plot that includes the datasets used in previous studies is shown in Fig. S19.

The model obtained by fitting previous datasets which takes into account the bedload transport saturation length (Lapotre et al., 2016) predicts significantly lower wavelengths and a different scaling to the one we derived from our dataset. Conversely, our data for the dark-toned large ripples overlaps the predictions of the wind-drag model that uses the saltation transport saturation length, with a best fitted power law with ~2/3 scaling.

Tharsis data presents higher scattering, particularly for lower wavelengths where data points seem to converge towards the dark-toned ripple dataset. Due to the discrepancies found between our results and those of Lorenz et al. (2014), we note that the Tharsis data compiled in this study does not overlap or follow a similar scaling to the wind-drag model that considers a bedload transport saturation length (Fig. 3 and S19). Instead, the best fitted power law (R^2=0.42) has the same scaling (~2/3) of the model that uses the saltation transport saturation length.

The compiled data suggests that the mechanism that limits the size of large ripples on Mars is dependent on the atmospheric density. Overall, we observe that all our data are bounded by the two saturation length scaling laws, supporting the hypothesis that the equilibrium size of large martian ripples is controlled by an aerodynamic mechanism. The scaling laws for saturation length arise from idealized representations of transport in unimodal sediments. As previously discussed, the grain size distribution of the sediments on the Tharsis bedforms is probably more complex, which may contribute to the observed differences between Tharsis and non-Tharsis bedforms.

Even so, in accordance with previous studies (Lorenz, 2020; Lorenz et al., 2014) we notice that linear functions (which imply that $\lambda \propto 1/\rho_f$) also provide robust fits to the data (R^2=0.79 and 0.73 for the dark large ripples and Tharsis bedforms, respectively). In the case of the large ripples, both inverse and power law functions explain ~80% of the variance. This means that, strictly from a numeric point of view, we cannot discriminate what is the best model to fit the data. As previously mentioned, to fully test the impact ripple hypothesis we would need to consider the wind velocities at each site, something that could be done using climate model predictions.

Finally, the wavelengths of the larger bedforms (megaripples and TARs) present a large dispersion (Fig. 3B), not showing an obvious relation with any of the scaling laws. Linear or power law models do not produce a meaningful fit to the data (R^2=0.03). This suggests that at a global scale these bedforms do not form a homogeneous set and are probably not representative of the same boundary conditions (i.e., they likely formed with different grain size distributions, or under differing atmospheric conditions). Nonetheless, we cannot exclude the possibility that including TARs and megaripples in a same class may be flawed, especially since different degrees of mobility under present day winds have been described for the two sets of bedforms (Chojnacki et al., 2021; Silvestro et al., 2020).

For the dark-toned large ripples the degree of agreement between the global measurements and the predictions of the scaling relationship of Lapotre et al. (2021) (where saturation length is taken as that of aeolian saltation) is remarkable. Particularly if we consider that we are using a "static" average atmospheric density, which is merely a function of elevation and does not consider regional and seasonal atmospheric density variations. On the other hand, we cannot exclude that the density may just be one of the factors influencing the bedforms dimensions. As suggested by Lorenz (2020), wind speed at a global scale may increase with elevation creating a more complex interplay between density, wind speed and resulting bedform size.

5 Conclusions

This survey provides improved measurements to evaluate the mechanisms that set the size of bedform on Mars. We show that previous works used biased measurements, particularly for the bedforms located in the Tharsis region. We investigated the uniqueness of the bedforms located in this region, concluding that these bedforms form a distinct population and should be analyzed separately from the more common dark-toned large ripples that cover dunes outside Tharsis.

Our survey covers a larger range of elevations than previous works, and for the first time provides full wavelength mapping of extensive regions. Overall, our results are consistent with the predictions of the "wind-drag" hypothesis, favoring the model that considers a saltation transport saturation length. Still, the compiled morphometric data is not enough to refute the impact ripple hypothesis, as that would probably require the integration of variable wind velocities for each site.

The compiled dataset corroborates the existence of a robust relation between the wavelength of large dark-toned ripples and atmospheric density. Therefore, this new survey complements and helps to validate the main concept introduced in Lapotre et al. (2016): that paleoatmospheric density can be inferred for Mars by looking at the aeolian sedimentary record, providing an important tool to probe the evolution of the planet's environment.

Acknowledgments

This research was supported by CITEUC (UID/Multi/00611/2021&POCI-01- 0145-FEDER-006922) and by FCT grant CEECIND/02981/2017. M. C. and S.S. were funded by NASA Mars Data Analysis Program Grant 80NSSC20K1066. We thank the Laboratory for Advanced Computing at University of Coimbra for providing computing resources.

We acknowledge the valuable comments and suggestions made by Mathieu Lapotre and two anonymous reviewers to an earlier version of this work. We thank Rob Sullivan for insights on the morphodynamics of impact ripples.

Open Research

HiRISE images used in this work are publicly available at the Planetary Data System (https://hirise-pds.lpl.arizona.edu/PDS/) where details can be obtained at McEwen et al. (2007). The morphometric database compiled in this study is available at https://doi.org/10.6084/m9.figshare.21064657.

References

Andreotti, B, Claudin, P., & Pouliquen, O. (2006). Aeolian sand ripples: Experimental study of fully developed states. *Physical Review Letters*, *96*(2). https://doi.org/Doi 10.1103/Physrevlett.96.028001

Andreotti, Bruno, Claudin, P., Iversen, J. J., Merrison, J. P., & Rasmussen, K. R. (2021). A lower-than-expected saltation threshold at Martian pressure and below. *Proceedings of the National Academy of Sciences of the United States of America*, *118*(5). https://doi.org/10.1073/pnas.2012386118

Bagnold, R. A. (1954). *The Physics of Blown Sand and Desert Dunes* (2nd ed.). New York: Dover Publications, INC.

Baker, M. M., Lapotre, M. G. A., Minitti, M. E., Newman, C. E., Sullivan, R., Weitz, C. M., et al. (2018). The Bagnold Dunes in Southern Summer: Active Sediment Transport on Mars Observed by the Curiosity Rover. *Geophysical Research Letters*, *45*(17), 8853–8863. https://doi.org/10.1029/2018GL079040

Baker, M. M., Newman, C. E., Sullivan, R., Minitti, M. E., Edgett, K. S., Fey, D., et al. (2022). Diurnal Variability in Aeolian Sediment Transport at Gale Crater, Mars. *Journal of Geophysical Research: Planets*, *127*(2), 1–27. https://doi.org/10.1029/2020JE006734

Bridges, N. T., Banks, M. E., Beyer, R. A., Chuang, F. C., Noe Dobrea, E. Z., Herkenhoff, K. E., et al. (2010). Aeolian bedforms, yardangs, and indurated surfaces in the Tharsis Montes as seen by the HiRISE Camera: Evidence for dust aggregates. *Icarus*, *205*(1), 165–182. https://doi.org/10.1016/j.icarus.2009.05.017

Bridges, N. T., Ayoub, F., Avouac, J.-P., Leprince, S., Lucas, a, & Mattson, S. (2012). Earth-like sand fluxes on Mars. *Nature*, *485*(7398), 339–42. https://doi.org/10.1038/nature11022

Cheng, H., Liu, C., Li, J., Liu, B., Zheng, Z., Zou, X., et al. (2018). Experimental study of aeolian sand ripples in a wind tunnel. *Earth Surface Processes and Landforms*, *43*(1), 312–321. https://doi.org/10.1002/esp.4246

Chojnacki, M., Vaz, D. A., Silvestro, S., & Silva, D. C. A. (2021). Widespread Megaripple Activity Across the North Polar Ergs of Mars. *Journal of Geophysical Research: Planets*, 1–19. https://doi.org/10.1029/2021je006970

Day, M., & Zimbelman, J. R. (2021). Ripples, megaripples, and TARs, Oh, My! Recommendations regarding Mars aeolian bedform terminology. *Icarus*, *369*, 114647. https://doi.org/10.1016/j.icarus.2021.114647

Duran Vinent, O., Andreotti, B., Claudin, P., & Winter, C. (2019). A unified model of ripples and dunes in water and planetary environments. *Nature Geoscience*, *12*(5), 345–350. https://doi.org/10.1038/s41561-019-0336-4

Fenton, L. K. (2020). Updating the global inventory of dune fields on mars and identification of many small dune fields. *Icarus*, *352*(May), 114018. https://doi.org/10.1016/j.icarus.2020.114018

Foroutan, M., & Zimbelman, J. R. (2017). Semi-automatic mapping of linear-trending bedforms using 'Self-Organizing Maps' algorithm. *Geomorphology*, *293*(May), 156–166. https://doi.org/10.1016/j.geomorph.2017.05.016

Gonzalez, R. C., Woods, R. E., & Eddins, S. L. (2004). *Digital Image processing using MATLAB*. Upper Saddle River, NJ: Pearson/Prentice Hall.

Gough, T. R., Hugenholtz, C. H., & Barchyn, T. E. (2021). Re-Evaluation of Large Martian Ripples in Gale Crater: Granulometric Evidence for an Impact Mechanism and Terrestrial Analogues. *Journal of Geophysical Research: Planets*, *126*(12). https://doi.org/10.1029/2021JE007011

Hayward, R. K., Fenton, L. K., & Titus, T. N. (2014). Mars Global Digital Dune Database (MGD3): Global dune distribution and wind pattern observations. *Icarus*, *230*, 38–46. https://doi.org/10.1016/j.icarus.2013.04.011

Kok, J. F. (2010). An improved parameterization of wind-blown sand flux on Mars that includes the effect of hysteresis. *Geophysical Research Letters*, *37*(12), 1–6. https://doi.org/10.1029/2010GL043646

Lapotre, M. G. A., Ewing, R. C., Lamb, M. P., Fischer, W. W., Grotzinger, J. P., Rubin, D. M., et al. (2016). Large wind ripples on Mars: A record of atmospheric evolution. *Science*, *353*(6294), 55–58. https://doi.org/10.1126/science.aaf3206

Lapotre, M. G. A., Ewing, R. C., Weitz, C. M., Lewis, K. W., Lamb, M. P., Ehlmann, B. L., & Rubin, D. M. (2018). Morphologic Diversity of Martian Ripples: Implications for Large-Ripple Formation. *Geophysical Research Letters*, *45*(19), 10,229-10,239. https://doi.org/10.1029/2018GL079029

Lapotre, Mathieu G.A., Lamb, M. P., & McElroy, B. (2017). What sets the size of current ripples? *Geology*, *45*(3), G38598.1. https://doi.org/10.1130/G38598.1

Lapotre, Mathieu G.A., Ewing, R. C., & Lamb, M. P. (2021). An Evolving Understanding of Enigmatic Large Ripples on Mars. *Journal of Geophysical Research: Planets*, *126*(2), 1–8. https://doi.org/10.1029/2020JE006729

Lorenz, R. D. (2020). Martian Ripples Making a Splash. *Journal of Geophysical Research: Planets*, *125*(10), 12–15. https://doi.org/10.1029/2020JE006658

Lorenz, R. D., Bridges, N. T., Rosenthal, A. A., & Donkor, E. (2014). Elevation dependence of bedform wavelength on Tharsis Montes, Mars: Atmospheric density as a controlling parameter. *Icarus*, *230*, 77–80. https://doi.org/10.1016/j.icarus.2013.10.026

Manukyan, E., & Prigozhin, L. (2009). Formation of aeolian ripples and sand sorting. *Physical Review E - Statistical, Nonlinear, and Soft Matter Physics*, *79*(3).

https://doi.org/10.1103/PhysRevE.79.031303

McEwen, A. S., Eliason, E. M., Bergstrom, J. W., Bridges, N. T., Hansen, C. J., Delamere, W. A., et al. (2007). Mars Reconnaissance Orbiter's High Resolution Imaging Science Experiment (HiRISE). *Journal of Geophysical Research-Planets*, *112*(E5). https://doi.org/Doi 10.1029/2005je002605

Moller, M. F. (1993). A Scaled Conjugate-Gradient Algorithm for Fast Supervised Learning. *Neural Networks*, *6*(4), 525–533. https://doi.org/Doi 10.1016/S0893-6080(05)80056-5

Putzig, N. E., & Mellon, M. T. (2007). Apparent thermal inertia and the surface heterogeneity of Mars. *Icarus*, *191*(1), 68–94. https://doi.org/10.1016/j.icarus.2007.05.013

Rasmussen, K. R., Valance, A., & Merrison, J. (2015). Laboratory studies of aeolian sediment transport processes on planetary surfaces. *Geomorphology*, *244*, 74–94. https://doi.org/10.1016/j.geomorph.2015.03.041

Ruff, S. W., & Christensen, P. R. (2002). Bright and dark regions on Mars: Particle size and mineralogical characteristics based on thermal emission spectrometer data. *Journal of Geophysical Research E: Planets*, *107*(12), 1–22. https://doi.org/10.1029/2001je001580

Sharp, R. P. (1963). Wind Ripples. *Journal of Geology*, *71*(5), 617–636. Retrieved from http://www.jstor.org/stable/30061128

Silvestro, S., Fenton, L. K., Vaz, D. A., Bridges, N. T., & Ori, G. G. (2010). Ripple migration and dune activity on Mars: Evidence for dynamic wind processes. *Geophysical Research Letters*, *37*(20), L20203. https://doi.org/Doi 10.1029/2010gl044743

Silvestro, S., Vaz, D. A., Ewing, R. C., Rossi, A. P., Fenton, L. K., Michaels, T. I., et al. (2013). Pervasive aeolian activity along rover Curiosity's traverse in Gale Crater, Mars. *Geology*, *41*(4), 483–486. https://doi.org/Doi 10.1130/G34162.1

Silvestro, S., Vaz, D. A., Yizhaq, H., & Esposito, F. (2016). Dune-like dynamic of Martian Aeolian large ripples. *Geophysical Research Letters*, *43*(16), 8384–8389. https://doi.org/10.1002/2016GL070014

Silvestro, S., Chojnacki, M., Vaz, D. A., Cardinale, M., Yizhaq, H., & Esposito, F. (2020). Megaripple Migration on Mars. *Journal of Geophysical Research: Planets*, *125*(8). https://doi.org/10.1029/2020JE006446

Smith, D. E., Zuber, M. T., Solomon, S. C., Phillips, R. J., Head, J. W., Garvin, J. B., et al. (1999). The Global Topography of Mars and Implications for Surface Evolution, *284*(May),

1495–1503.
Soille, P. (2002). *Morphological Image Analysis - Principles and Applications*. Berlin: Springer-Verlag.
Sullivan, R., & Kok, J. F. (2017). Aeolian saltation on Mars at low wind speeds. *Journal of Geophysical Research: Planets*, *122*(10), 2111–2143. https://doi.org/10.1002/2017JE005275
Sullivan, R., Kok, J. F., Katra, I., & Yizhaq, H. (2020). A Broad Continuum of Aeolian Impact Ripple Morphologies on Mars is Enabled by Low Wind Dynamic Pressures. *Journal of Geophysical Research: Planets*, *125*(10), 1–39. https://doi.org/10.1029/2020je006485
Sullivan, R., Baker, M., Newman, C., Turner, M., Schieber, J., Weitz, C., et al. (2022). The Aeolian Environment in Glen Torridon, Gale Crater, Mars. *Journal of Geophysical Research: Planets*, *127*(8), 1–39. https://doi.org/10.1029/2021JE007174
Swann, C., Sherman, D. J., & Ewing, R. C. (2020). Experimentally Derived Thresholds for Windblown Sand on Mars. *Geophysical Research Letters*, *47*(3), 1–10. https://doi.org/10.1029/2019GL084484
Taubman, D. S., & Marcellin, M. W. (2002). JPEG2000: Standard for interactive imaging. *Proceedings of the IEEE*, *90*(8), 1336–1357. https://doi.org/10.1109/JPROC.2002.800725
Vaz, D. A., & Silvestro, S. (2014). Mapping and characterization of small-scale aeolian structures on Mars: An example from the MSL landing site in Gale Crater. *Icarus*, *230*, 151–161.
Vaz, D. A., Sarmento, P. T. K., Barata, M. T., Fenton, L. K., & Michaels, T. I. (2015). Object-based Dune Analysis: Automated dune mapping and pattern characterization for Ganges Chasma and Gale crater, Mars. *Geomorphology*, *250*, 128–139. https://doi.org/10.1016/j.geomorph.2015.08.021
Vaz, D. A., Silvestro, S., Sarmento, P. T. K., & Cardinale, M. (2017). Migrating meter-scale bedforms on Martian dark dunes: Are terrestrial aeolian ripples good analogues? *Aeolian Research*, *26*, 101–116. https://doi.org/10.1016/j.aeolia.2016.08.003
Voulgaris, G., & Morin, J. P. (2008). A long-term real time sea bed morphology evolution system in the South Atlantic Bight. *Proceedings of the Ieee/Oes/Cmtc Ninth Working Conference on Current Measurement Technology*, 71–79.
Weitz, C. M., Sullivan, R. J., Lapotre, M. G. A., Rowland, S. K., Grant, J. A., Baker, M., &

Yingst, R. A. (2018). Sand Grain Sizes and Shapes in Eolian Bedforms at Gale Crater, Mars. *Geophysical Research Letters*, *45*(18), 9471–9479. https://doi.org/10.1029/2018GL078972

Withers, P., & Smith, M. D. (2006). Atmospheric entry profiles from the Mars Exploration Rovers Spirit and Opportunity. *Icarus*, *185*(1), 133–142. https://doi.org/10.1016/j.icarus.2006.06.013